Dual weighted a posteriori error estimation for a new nonconforming linear finite element on quadrilaterals

Matthias Grajewski and Jaroslav Hron and Stefan Turek

Institute of Applied Mathematics, University of Dortmund, Vogelpothsweg 87, D-44227 Dortmund, Germany,
Matthias.Grajewski@mathematik.uni-dortmund.de

Abstract

After a short introduction of a new nonconforming linear finite element on quadrilaterals recently developed by Park, we derive a dual weighted residual-based a posteriori error estimator (in the sense of Becker and Rannacher) for this finite element. By computing a corresponding *dual solution* we estimate the error with respect to a given target error functional. The reliability and efficiency of this estimator is analyzed in several numerical experiments.

1 Introduction

For the numerical treatment of partial differential equations (PDEs), especially in the simulation of incompressible flow, nonconforming finite element methods play an important role. The advantages of these elements are their (often) excellent stability properties with respect to the 'inf-sup-condition' ("LBB-stable") and to anisotropic mesh deformations, together with the possibility to provide highly efficient solvers with discrete projection techniques or Pressure-Schur-Complement methods for nonstationary problems (see c.f. [12]). This makes them a good choice for a high performance simulation tool. Moreover, their mostly edge-oriented degrees of freedom lead to very compact data structures which have special advantages for parallel high-performance computations [5]. Altogether, they are quite natural candidates to combine modern error control mechanisms and concepts for adaptivity in space and time with optimized high performance computing techniques to simulate realistic problems, in particular for *Computational Fluid Dynamics* (CFD). In the case of the incompressible Stokes- or Navier-Stokes equations the element pair (E_1, E_2), where E_1 discretizes the velocities and E_2 the pressure, is

sometimes called 'Stokes-element'. Examples of popular Stokes-elements are the pairs (Q_1, Q_0) (conforming bilinear velocity, piecewise constant pressure), (Q_1, Q_1) (conforming bilinear velocity and pressure), (Q_2, P_1^{disc}) (conforming biquadratic velocity, discontinuous linear pressure), (P_1^{nc}, P_0) (nonconforming linear velocity, piecewise constant pressure), $(\tilde{Q}_1, Q_0)$ (nonconforming rotated bilinear velocity, piecewise constant pressure) and many more.
There is still an ongoing research for new and more efficient, accurate and robust discretisations for such saddle-point problems. The combination of the new element proposed in this article together with a piecewise constant pressure turns out *not to be LBB-stable* similar to the very popular (Q_1, Q_0) Stokes-element, but because of its simple structure (it is in fact the simplest nonconforming quadrilateral element known besides a piecewise constant approach) it plays the role of a new prototypical nonconforming finite element and merits therefore attention.
Let Ω be a bounded 2-dimensional domain with polygonal boundary (we restrict ourselves to 2D for technical reasons only), and let $\partial\Omega$ denote the boundary of Ω. Furthermore, let $\mathcal{P}_k$ be the polynomial space with maximum total degree k and $\mathcal{Q}_k$ the polynomial space with maximum degree k in each variable. The L^2-scalar product on Ω is denoted by $(\cdot,\cdot)$, the corresponding L^2-norm by $||\cdot||$ and the usual Sobolev norms by $||\cdot||_m, m \geq 1$.
C. Park introduced in his PhD-thesis [9] and in [10] a linear quadrilateral nonconforming finite element which is called $\tilde{P}_1$ in this article. Let $\mathbb{T}_h$ denote a conforming mesh over a polygonal domain Ω, which shall consist of convex quadrilaterals, and $\partial\mathbb{T}_h$ the set of all edges of $\mathbb{T}_h$. According to our setting, we have $\bar{\Omega} = \bigcup_{T\in\mathbb{T}_h} T$. The construction of the element and the corresponding finite element space $\tilde{P}_1(\mathbb{T}_h)$ relies on the following simple facts. By elementary (vector) calculus one proves for an arbitrary convex quadrilateral T with vertices $v_1, \ldots, v_4$ and edge midpoints $m_1, \ldots, m_4$ that these midpoints form a parallelogram. Exploiting this fact, one can show [7,9] that

$$\forall\, u \in \mathcal{P}_1(T) : u(m_1) + u(m_3) = u(m_2) + u(m_4) \tag{1}$$

and, vice versa,

$$\forall\, u_1, \ldots u_4 \text{ with } u_1 + u_3 = u_2 + u_4 \;\; \exists! u \in \mathcal{P}_1(T) :\; u_i = u(m_i). \tag{2}$$

Here we assume the vertices and midpoints of the edges to be orderd as in Figure 1. This allows the following definition:

Definition 1.1 (Park) 1) *Let v_j be an arbitrary vertex in $\mathbb{T}_h$ and $\mathcal{M}(j) := \{i \in \mathbb{N} \,\big|\, \exists\Gamma \in \partial\mathbb{T}_h : m_i \in \Gamma \wedge v_j \in \Gamma\}$ "the neighbourhood of v_j". Then we can define Φ_j by $\Phi_j|_T \in \mathcal{P}_1(T)\,\forall\, T \in \mathbb{T}_h$ and*

$$\Phi_j(m_i) := \begin{cases} 1 & , \quad i \in \mathcal{M}(j) \\ 0 & , \quad \textit{else} \end{cases} \tag{3}$$

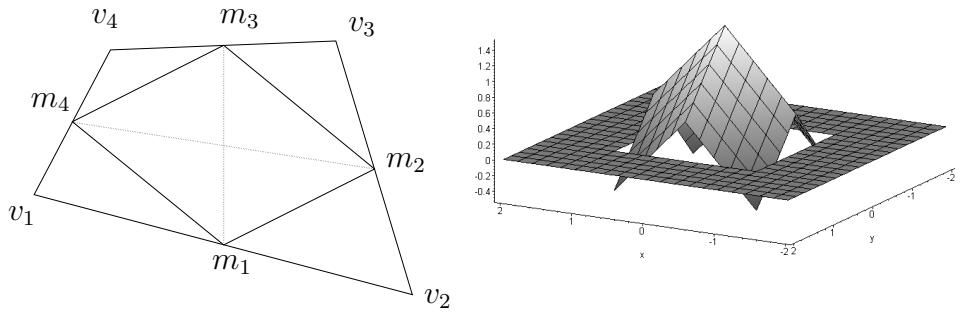

Fig. 1. Edge midpoints of an arbitrary quadrilateral form a parallelogram; $\tilde{P}_1$ basis function Φ_j at node v_j

2) *The finite element space* $\tilde{P}_1(\mathbb{T}_h)$ *is defined by*

$$\tilde{P}_1(\mathbb{T}_h) := \left\{ \varphi : \Omega \to \mathbb{R} \;\middle|\; \varphi|_T \in \mathcal{P}_1(T) \,\forall\, T \in \mathbb{T}_h \wedge \varphi \text{ continuous in } m_\Gamma \,\forall\, \Gamma \right\}, \tag{4}$$

where m_Γ *denotes the midpoint of the edge* $\Gamma \in \partial\mathbb{T}$.

Let $||\cdot||_{1,h}$ denote the discrete H^1-norm defined by $||\cdot||_{1,h} := (\sum_{T\in\mathbb{T}_h} ||\cdot||_1^2)^{1/2}$. For the finite element space $\tilde{P}_1(\mathbb{T}_h)$ there holds the typical FEM approximation result:

Theorem 1 (Park [9,10]) 1) *Let* $\Omega \subset \mathbb{R}^2$ *be a simply connected convex domain with piecewise polygonal boundary. The triangulation* $\mathbb{T}_h$ *shall contain* N *vertices. Furthermore, to each inner edge, there shall belong at least one inner vertex. Then,*

$$\dim \tilde{P}_1(\mathbb{T}_h) = N - 1. \tag{5}$$

For arbitrary $0 < \hat{\jmath} \leq N$, *the set* $\{\Phi_j \mid j \in \{1 \ldots, N\} \setminus \{\hat{\jmath}\}\}$ *forms a basis of* $\tilde{P}_1(\mathbb{T}_h)$.
2) *Let* $f \in L^2(\Omega)$, $g \in H^{\frac{1}{2}}(\partial\Omega)$ *and* u *the solution of the Robin boundary value problem*

$$a(u,\varphi) := (\nabla u, \nabla\varphi)_\Omega + (cu,\varphi)_\Omega + (u,\varphi)_{\partial\Omega} = (f,\varphi)_\Omega + (g,\varphi)_{\partial\Omega} \quad \forall\, \varphi \in H^1(\Omega). \tag{6}$$

Then, there is a constant C *not depending on* h, *such that*

$$||u - u_h||_0 + h||u - u_h||_{1,h} \leq Ch^2||u||_2 \tag{7}$$

holds for the discrete solution u_h.

For a tensor product mesh, a typical basis function Φ_j is displayed in Figure 1 (right). It is crucial that the finite element space $\tilde{P}_1(\mathbb{T}_h)$ is not necessarily obtained by a parametric transformation from some reference element, although it is possible to define such a finite element space. As in the case of the rotated bilinear $\tilde{Q}_1$-approach (see [13]) there arise problems for distorted meshes

(compare also [1]). Numerical experiments show that in the case of the Poisson problem the H^1- and L^2-errors for this nonparametric $\tilde{P}_1$ are comparable to the errors obtained with computations with the conforming Q_1-element or the nonconforming $\tilde{Q}_1$-element. For details concerning the transformation procedure, solver aspects and efficient matrix assembly as well as numerical results for $\tilde{P}_1$, we refer to [7,10].

Besides an accurate and stable discretisation, error control and adaptivity are essential ingredients for creating a simulation tool which can solve real-world problems in reasonable time. Especially in 3D, it is virtually impossible to perform "brute force" calculations, i.e. taking a coarse mesh and refining regularly until the solution seems to be approximated well enough. Deciding whether the solution is sufficiently accurate or not is particularly difficult in practical applications, as one is often not interested in the overall solution but in derived quantities like lift or drag. Therefore, a posteriori error estimation with respect to H^1- or L^2-norm only, as many papers deal with, is often of only limited practical use. In contrast to this, Becker and Rannacher introduced in the case of conforming finite elements a posteriori error estimation with respect to a given *output functional* J [2,3]. Their method relying on computing a suitable *dual problem* has proven to be very successful in several applications. Unfortunately, there is much less literature concerning such error estimation in the nonconforming case (see e.g. [8,11]). The main topic of this paper is to make a contribution to fill this gap in the special case of the new nonconforming element $\tilde{P}_1$.

2 Dual weighted a posteriori error control for $\tilde{P}_1$

As discussed in the introduction, error estimation with respect to global norms does not seem to be favourable in many practical computations. Instead of this, one is often interested in the error of derived quantities. The evaluation of these quantities can be expressed by applying an *output functional* J to the solution. Examples of such functionals are

$$J_{x_0}(\varphi) = \varphi(x_0) \tag{8}$$

which describes the measurement of the point value in x_0 and

$$J_\Gamma(\varphi) = \int_\Gamma \partial_{\mathfrak{n}}\varphi \, ds \tag{9}$$

which is related to evaluating boundary integrals of derivatives on $\Gamma \subset \partial\Omega$, for instance the Nusselt number. Therefore, performing a posteriori error control with respect to an output functional J means finding an upper (and lower)

bound for

$$|J(u) - J(u_h)|,$$

whre u and u_h are the continuous and discrete solution of the underlying PDE. In this paper, we consider as prototype for an elliptic problem the Poisson equation

$$-\Delta u = f \tag{10}$$

with homogeneous Dirichlet conditions. Before tackling the nonconforming case, we will review the conforming case in the sense of Becker and Rannacher to clarify the problems arising for nonconforming finite elements and to show the differences and relations of the conforming and nonconforming case.
Let for the sake of simplicity J be a linear and continuous functional. We start with the standard variational formulation of the Poisson equation for the solution $u \in H_0^1(\Omega)$

$$a(u, \varphi) := (\nabla u, \nabla \varphi) = (f, \varphi) \quad \forall \varphi \in V := H_0^1(\Omega) \tag{11}$$

and its discrete analogon

$$a(u_h, \varphi_h) = (f, \varphi_h) \quad \forall \varphi_h \in V_h, \tag{12}$$

where V_h denotes a suitable FEM-subspace of V. According to Becker and Rannacher we define the corresponding dual problem with dual solution $z \in V$

$$(\nabla \varphi, \nabla z) = J(\varphi) \quad \forall \varphi \in V \tag{13}$$

and the corresponding discrete version

$$(\nabla \varphi_h, \nabla z_h) = J(\varphi_h) \quad \forall \varphi_h \in V_h. \tag{14}$$

In the conforming case, i.e. in the case $V_h \subset V$, there holds the fundamental Galerkin orthogonality

$$a(u - u_h, \varphi_h) = a(z - z_h, \varphi_h) = 0 \quad \forall \varphi \in V_h. \tag{15}$$

Using these ingredients and Green's formula, we derive with the abbreviation $e_h := u - u_h$ the error representation

$$\begin{aligned}
|J(e_h)| &= |a(z, e_h)| \\
&\overset{(15)}{=} |a(u - u_h, z - \varphi_h)| \\
&= \left| \sum_{T \in \mathbb{T}_h} (\nabla(u - u_h), \nabla(z - \varphi_h))_T \right| \qquad (16) \\
&= \left| \sum_{T \in \mathbb{T}_h} \left\{ (f + \Delta u_h, z - \varphi_h)_T - \frac{1}{2}([\partial_{\mathfrak{n}} u_h], z - \varphi_h)_{\partial T} \right\} \right|. \qquad (17)
\end{aligned}$$

As usual, the term $[\cdot]$ denotes the *jump* across an element edge.
In the more general situation

$$-\Delta u = f, \quad u|_{\partial\Omega_D} = u_D, \quad \partial_{\mathfrak{n}} u|_{\partial\Omega_N} = g$$

with Ω having a polygonal boundary $\partial\Omega = \partial\Omega_D \cup \partial\Omega_N$, where $\partial\Omega_D$ denotes the Dirichlet part of the boundary and $\partial\Omega_N$ the Neumann part, we can obtain by a slightly more sophisticated but similar derivation the error representation:

$$|J(e_h)| = \Big| \sum_{T\in\mathbb{T}_h} \Big\{ (f + \Delta u_h, z - \varphi_h)_T - \frac{1}{2}([\partial_{\mathfrak{n}} u_h], z - \varphi_h)_{\partial T} + (g, z - \varphi_h)_{\partial T \cap \partial\Omega_N} + (u_D - u_{D,h}, \partial_{\mathfrak{n}} z)_{\partial T \cap \partial\Omega_D} \Big\} \Big| \quad (18)$$

Here, $u_{D,h}$ is a suitable approximation of the given Dirichlet boundary data u_D in the finite element space V_h (for more details see a forthcoming paper). The error representation (18) incorporates in contrast to the former one (17) the error contributions of the approximations of the given boundary data.

In the nonconforming case, i.e. in the case of $V_h \not\subset V$, we can derive a formula similar to (17). If the error functional J is linear and continuous in $L^2(\Omega)$, there is according to Riesz's theorem a unique $j \in L^2(\Omega)$ with

$$J(\varphi) = (j, \varphi) \quad \forall \varphi \in L^2(\Omega).$$

As typically (see for instance [8]), we start with the assumption that there is a unique solution z of the dual problem

$$\Delta z = j, \quad z|_{\partial\Omega} = 0. \quad (19)$$

Testing with functions in $L^2(\Omega)$ leads to the variational formulation

$$(-\Delta z, \varphi) = (j, \varphi) \quad \forall \varphi \in L^2(\Omega). \quad (20)$$

Similar to the conforming case we derive by applying Green's formula the following error representation:

$$\begin{aligned} |J(e_h)| &= |(-\Delta z, u - u_h)| \\ &= \Big| \sum_{T\in\mathbb{T}_h} (\nabla(u - u_h), \nabla z)_T - (u - u_h, \partial_{\mathfrak{n}} z)_{\partial T} \Big| \\ &= \Big| \sum_{T\in\mathbb{T}_h} \Big\{ (z, f + \Delta u_h)_T - (\partial_{\mathfrak{n}} u_h, z)_{\partial T} - (u - u_h, \partial_{\mathfrak{n}} z)_{\partial T} \Big\} \Big| \end{aligned} \quad (21)$$

To insert φ_h, we need in the derivation of eq. (16) an analogon to the Galerkin orthogonality (15). As for any nonconforming method, there only holds a

reduced Galerkin orthogonality $a(u-u_h,\varphi_h)=0\,\forall\varphi_h\in V_h^C:=V_h\cap V$ in the case of a discretisation with $\tilde{P}_1$. In the case of $V_h=\tilde{P}_1$, the subspace V_h^C is too small to find any reasonable approximation z_h^C of z in it. Therefore, we modify the finite element space $\tilde{P}_1$ according to Suttmeier and Kanschat [8] by adding a *bulb function* φ_B which is defined by

$$\varphi_B(x,y)=xy$$

on the reference element $T_{\text{ref}}:=[-1,1]^2$. On any element, it holds $\varphi_B=0$ in the midpoints, therefore the continuity conditions of the finite element space are not touched by the enhancement. The bulb function is transformed parametrically in contrast to the other basis functions. By this, the finite element space V_h is augmented to a new finite element space $V_h^E:=\text{span}\{V_h,\{\varphi_B\}\}$. This augments also the conforming subspace V_h^C to the space $V_h^{E,C}$ to have appropriate approximation properties also in $V_h^{E,C}:=V\cap V_h^E$. In fact, $V_h^{E,C}$ equals the conforming space of parametric elementwise bilinear functions: As $V_h^{E,C}\subset V$, the functions in $V_h^{E,C}$ are continuous along the element edges and, in the case of an orthogonal mesh, the function space $V_h^{E,C}(T)$ on a single element T incorporates the functions $1,x,y$ from V_h^C and xy from the enhancement. Therefore, there holds $\text{span}\{1,x,y,xy\}=Q_1(T)\subset V_h^{E,C}(T)\,\forall T\in\mathbb{T}_h$ and consequently $Q_1\subset V_h^{E,C}$. On the other hand, $V_h^{E,C}\subset Q_1$ is obvious on orthogonal meshes and we obtain $V_h^{E,C}=Q_1$. On general meshes, one can argue analogously exploiting that φ_B is transformed *parametrically*. Then, there holds the modified Galerkin orthogonality

$$a_h(u-u_h^E,\varphi_h^C):=\sum_{T\in\mathbb{T}_h}(\nabla(u-u_h^E),\nabla\varphi_h^C)_T=0\quad\forall\varphi_h^C\in V_h^{E,C},\tag{22}$$

where u_h^E denotes the solution of the discrete problem in the enhanced space V_h^E. Hence, we can insert now some discrete function $\varphi_h^C\in V_h^{E,C}$ analogously to the conforming case. By applying Green's theorem and incorporating the definition of $a_h(\cdot,\cdot)$ in (22), we obtain from (21) the final error representation:

$$\begin{aligned}
J(e_h)&=(-\Delta e_h,z)\\
&=\sum_{T\in\mathbb{T}_h}(\nabla e_h,\nabla z)_T-(e_h,\partial_{\mathfrak{n}}z)_{\partial T}\\
&=a_h(e_h,z)-\sum_{T\in\mathbb{T}_h}(e_h,\partial_{\mathfrak{n}}z)_{\partial T}\\
&=a_h(e_h,z-\varphi_h^C)-\sum_{T\in\mathbb{T}_h}(e_h,\partial_{\mathfrak{n}}z)_{\partial T}+a_h(e_h,\varphi_h^C)\\
&=\sum_{T\in\mathbb{T}_h}\Big\{\left(f+\Delta u_h,z-\varphi_h^C\right)_T-\frac{1}{2}\left([\partial_{\mathfrak{n}}u_h],z-\varphi_h^C\right)_{\partial T}\\
&\qquad\qquad-\frac{1}{2}\left([u_h],\partial_{\mathfrak{n}}z\right)_{\partial T}\Big\}+a_h(e_h,\varphi_h^C)
\end{aligned}\tag{23}$$

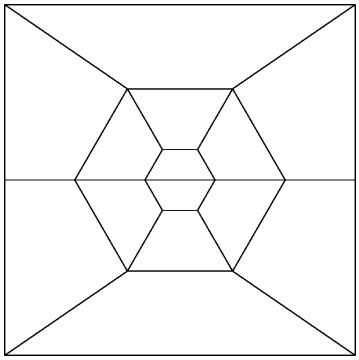

Fig. 2. Coarse grid for Test Problem 2.1

Here, the jump terms are defined as in the conforming case. The new consistency error $a_h(e_h, \varphi_h^C)$ occurs from taking u_h in V_h instead of u_h^E in V_h^E.

For an arbitrary function $\varphi(x, y) = a + bx + cy \in \tilde{P}_1(T_{\text{ref}})$, we get

$$(\varphi, \varphi_B)_{T_{\text{ref}}} = \int_{-1}^{1} \int_{-1}^{1} (a + bx + cy)xy \, dx \, dy = 0 \tag{24}$$

and, noting $\nabla\varphi = (b, c)^\top$,

$$(\nabla\varphi, \nabla\varphi_B)_{T_{\text{ref}}} = \int_{-1}^{1} \int_{-1}^{1} \begin{pmatrix} b \\ c \end{pmatrix} \cdot \begin{pmatrix} y \\ x \end{pmatrix} dx \, dy = 0$$

on the reference element T_{ref}. This orthogonality property remains true for any mesh consisting of parallelograms. In this case, the transformation Ψ from the reference element to the actual element T is linear and does not differ from the mapping used in the nonparametric transformation except of a scaling factor. Furthermore, the Jacobian $D\Psi$ of Ψ is constant. Therefore we obtain due to the area formula

$$(\varphi, \varphi_B)_T = c \det D\Psi \int_{[-1,1]^2} \Big((\varphi \circ \Psi^{-1}) \cdot (\varphi_B \circ \Psi^{-1}) \Big) \circ \Psi dx dy = C(\varphi, \varphi_B)_{T_{\text{ref}}} = 0.$$

An analogous argument holds for $(\nabla\varphi, \nabla\varphi_B)_T$. Therefore, we have the orthogonality relation

$$(\nabla\varphi_i, \nabla\varphi_B)_T = (\varphi_i, \varphi_B)_T = 0, \tag{25}$$

where φ_i are the basis functions of $\tilde{P}_1(T)$ and T is a parallelogram shaped element. However, on arbitrary quadrilaterals it is not known yet wether the orthogonality property (25) holds. On grids consisting of parallelograms, due to the orthogonality in (25), the discrete solution u_h^E in the enhanced space can be decoupled as

$$u_h^E = u_h + u_h^B$$

and we obtain by straightforward calculation for the consistency error

$$a_h(e_h, \varphi_h^C) = a_h(u_h^B, \varphi_h^B) \quad \forall \varphi_h^C \in V_h^{E,C}, \tag{26}$$

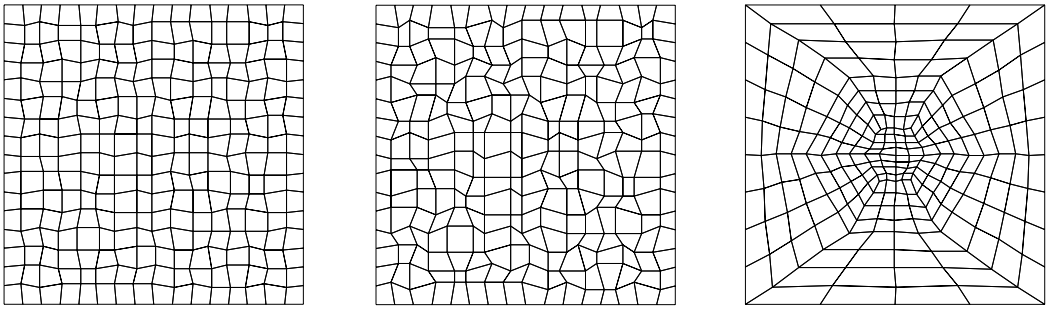

Fig. 3. Tensor product mesh ($h = 1/17$) with 10 % (left) and 20 % distortion (middle), grid from Fig. 2 after refinement ($h = 4.5 \cdot 10^{-2}$) and 4 % distortion

where φ_h^B denotes the bulb part of φ_h^C. Analogously to [8] one concludes $|a_h(e_h, \varphi_h^B)| = \mathcal{O}(h^4)$ on orthogonal meshes. Again, on arbitrary meshes there is no theoretical evidence that this statement is valid. To verify $|a_h(e_h, \varphi_h^B)| = \mathcal{O}(h^4)$ on regular meshes and to investigate the order of the consistency error in the case of more general ones, we examine

Test Problem 2.1 *For $\Omega = [0,1]^2$, f is chosen such that*

$$-\Delta u = f, \quad u|_{\partial\Omega} \equiv 0$$

is fulfilled by $u = x(x-1)y^2(1-y)\sin(x+2y)$.

Test Problem 2.1 is computed both on an equidistant tensor product mesh and the mesh displayed in Figure 2. The desired output quantity is the point error in $(0.5, 0.5)$ and the functional J_Γ, Γ being the boundary of the square. The regular refinement we use implies that by this refinement procedure the elements assume parallelogram shape asymptotically. To give results for more unstructured meshes, we additionally show computations of the consistency error on meshes which are distorted *after* regular refinement (see Fig. 3). The distortion is achieved as follows: Firstly, we refine the given coarse grid regularly up to the desired level of refinement. After this we compute a global element size $h := 1/\sqrt{\mathrm{NVT}}$, NVT is the number of grid points, of this refined mesh and modify the positions of the nodes by distortions of size $c \cdot h$. Here, the distortion parameter c is given in percent.
For φ_h^C, we have chosen a conforming approximation z_h^C of z which is computed as follows: We solve the dual problem (20) in the same space as the primal problem, i.e. by taking the $\tilde{P}_1$-element. The nonconforming discrete dual solution z_h is then projected into the conforming space formed by Q_1 by applying an angle weighted interpolation. Let $\mathcal{N}(j) := \{i \in \mathbb{N} \mid \mathbb{T}_h \ni T_i \cap v_j \neq \emptyset\}$ denote the neighbourhood of the j-th vertex and α_i the opening angles of the elements meeting in v_j. We set

$$z_h^C(v_j) := \sum_{i \in \mathcal{N}(j)} \frac{\alpha_i}{2\pi} \lim_{T_i \ni x \to v_j} z_h(x). \tag{27}$$

Then, z_h^C is defined by (parametric) bilinear interpolation of these values. By this method, we neither perform computations in $V_h^{E,C}$ nor in V_h^E but only in $\tilde{P}_1$. In the same way like the interpolation, the regularized functional $J_{x_0}^r$ is defined as

$$J_{x_0}^r(\varphi_h) := J_{x_0}(\varphi_h^C). \tag{28}$$

Note that direct interpolation as well as direct point evaluation is not possible as functions in V_h are discontinuous in the vertices.

The results of these computations are collected in Tables 1 and 2 (NEL = number of elements). They confirm $|a(e_h, z_h^C)| = \mathcal{O}(h^4)$ for tensor product grids as well as (at least) $\mathcal{O}(h^3)$ for arbitrary meshes which are refined regularly regardless of the output functional used. However, the consistency error does not seem to be of fourth order in the case of distorted meshes. The reduction factors in our experiments vary, but there is some evidence that in this case the consistency error seems to behave like $\mathcal{O}(h^3)$. Therefore we can assume that the consistency error will asymptotically vanish with respect to the other error contributions and will be therefore neglected from now on. Here, the order of the consistency error does not depend on the interpolation applied. Similar results are observed for an unweighted interpolation procedure or for area-weighted interpolation. It is also possible to define z_h^C as L^2-projection instead; experiments show that there is no substantial difference in these two projection types with respect to the consistency error (compare [6]).

However, the order of the consistency error seems to depend on the boundary treatment chosen. The boundary treatment proposed by Park in [9,10] only works fine in the case of simply connected domains. In the case of multiply connected domains, one observes a detoriation of convergence. Therefore we proposed a so-called implicit boundary treatment which performs well on arbitrary domains (for details see [6,7]). Unfortunately, it turns out that this kind of boundary treatment affects the consistency error and makes it to be of only second order. To demonstrate this, we computed the consistency error on the tensor product grid previously used, but with the implicit boundary treatment and the error functional J_Γ (see Table 3). Whenever the domain is simply connected, we use in this paper the explicit boundary treatment (except of Table 3). In contrast to this, whenever the domain is multiply connected, we apply the implicit boundary treatment. Nevertheless, the phenomenon described here only occurs in the case of the evaluation of J_Γ; if we estimate the point error of some interior point, we observe the consistency error to be of at least third order regardless of the boundary treatment. As there holds $J_\Gamma(e_h) = \mathcal{O}(h)$ because of the evaluation of incorporated derivatives, the second order consistency error can be neglected also in this case, independently of the boundary treatment chosen.

Remark 2.2 *In the final error representation, the conforming case appears as a special case of the nonconforming one. If the discrete solution u_h is continuous, the jump term $[u_h]$ will vanish on every inner element edge Γ, and therefore the terms $([u_h], \partial_{\mathfrak{n}} z)_\Gamma$ will vanish for all inner element edges.*

NEL	$\left\|a_h(e_h, z_h^C)\right\|$	red.	$\left\|a_h(e_h, z_h^C)\right\|$	red.	$\left\|a_h(e_h, z_h^C)\right\|$	red.
64	$3.54 \cdot 10^{-6}$	–	$1.93 \cdot 10^{-6}$	–	$5.65 \cdot 10^{-7}$	–
256	$1.80 \cdot 10^{-7}$	19.7	$1.35 \cdot 10^{-7}$	14.3	$6.18 \cdot 10^{-7}$	0.91
1024	$1.07 \cdot 10^{-8}$	16.8	$9.83 \cdot 10^{-8}$	13.7	$2.26 \cdot 10^{-7}$	2.73
4096	$6.65 \cdot 10^{-10}$	16.1	$1.14 \cdot 10^{-8}$	8,62	$2.40 \cdot 10^{-8}$	9.42
16384	$4.14 \cdot 10^{-11}$	16.1	$9.81 \cdot 10^{-10}$	11.6	$1.66 \cdot 10^{-9}$	14.5
65536	$2.61 \cdot 10^{-12}$	15.9	$9.67 \cdot 10^{-11}$	10.1	$1.22 \cdot 10^{-10}$	13.6

Table 1
Consistency error $\left|a_h(e_h, z_h^C)\right|$ on a regularly refined tensor product grid (left) and on tensor product grids with 10 % (middle) and 20 % distortion (right), Test Problem 2.1, dual solution z to estimate the point error in $(\frac{1}{2}, \frac{1}{2})$

	z to estimate point error in $(\frac{1}{2}, \frac{1}{2})$				z to estimate $J_\Gamma(e_h)$			
NEL	$\left\|a_h(e_h, z_h^C)\right\|$	red.	$\left\|a_h(e_h, z_h^C)\right\|$	red.	$\left\|a_h(e_h, z_h^C)\right\|$	red.	$\left\|a_h(e_h, z_h^C)\right\|$	red.
56	$3.05 \cdot 10^{-4}$	–	$3.07 \cdot 10^{-4}$	–	$5,37 \cdot 10^{-3}$	–	$5.24 \cdot 10^{-3}$	–
224	$1.27 \cdot 10^{-5}$	24.0	$1.40 \cdot 10^{-5}$	21.9	$4,26 \cdot 10^{-4}$	12.6	$4.84 \cdot 10^{-4}$	10.8
896	$8.00 \cdot 10^{-7}$	15.9	$9.48 \cdot 10^{-7}$	14.8	$7,17 \cdot 10^{-5}$	5.94	$8.31 \cdot 10^{-5}$	5.82
3584	$5.10 \cdot 10^{-8}$	15.7	$5.90 \cdot 10^{-8}$	16.1	$9.33 \cdot 10^{-6}$	7.68	$9.83 \cdot 10^{-6}$	8.45
14336	$3.23 \cdot 10^{-9}$	15.8	$3.84 \cdot 10^{-9}$	15.4	$1.01 \cdot 10^{-6}$	9.24	$1.04 \cdot 10^{-6}$	9.45
57344	$2.04 \cdot 10^{-10}$	15.8	$2.69 \cdot 10^{-10}$	14.3	$9.55 \cdot 10^{-8}$	10.6	$9.38 \cdot 10^{-8}$	11.1

Table 2
Consistency error $\left|a_h(e_h, z_h^C)\right|$ on the grid shown in Figure 2 resp. 3 without (1st and 3rd column) and with 4 % distortion (2nd and 4th column), Test Problem 2.1

NEL	$\left\|a_h(e_h, z_h^C)\right\|$	red.
64	$1.86 \cdot 10^{-3}$	–
256	$4.54 \cdot 10^{-4}$	4.10
1024	$1.13 \cdot 10^{-4}$	4.02
4096	$2.82 \cdot 10^{-5}$	4.00
16384	$7.04 \cdot 10^{-6}$	4.01
65536	$1.76 \cdot 10^{-6}$	4.00

Table 3
Consistency error $\left|a_h(e_h, z_h^C)\right|$ on a regularly refined tensor product grid, dual solution z to estimate $J_\Gamma(e_h)$ including normal derivatives on $\partial\Omega$, implicit boundary treatment.

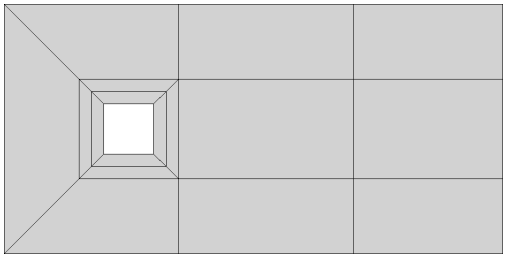

Fig. 4. Grid for 'square in a channel'

3 Implementation and numerical results

The error representations (16) and (21), although being exact, cannot be directly evaluated in practical calculations, as the dual solution z is unknown as well as the primal solution u. Therefore, one will replace z by a suitable discrete approximation $\tilde{z}$. As a consequence, the error representations (16) and (21) become error estimations. The term 'estimation' in this context does not imply to have a strict upper bound for the true error. To obtain asymptotic exactness of the error estimation, the replacement error $||z - \tilde{z}||_1$ should be of higher order than $||u - u_h||_1$. This can be achieved for example by special postprocessing of z_h obtaining superconvergence properties. Unfortunately, these properties usually rely on tensor product meshes. Therefore, one might use higher order elements in practice, which can imply unacceptably high costs for computing the dual problem. However, for finding a balance between the accuracy of $\tilde{z}$ and the computational amount of its computation, there is no fixed rule. Often, one will restrict to the condition $||z - \tilde{z}||_1 \ll ||z - z_h||_1$. By this, asymptotic exactness cannot be expected any more.
The latter requirement can e.g. be fulfilled by an interpolation approach analogous to the conforming case ([2,3]). Here, $\tilde{z}$ is defined as a biquadratic interpolation with interpolation nodes being the vertices on a patch consisting of four elements. This patchwise interpolation will be referred to as z^I from now on. To proceed exactly the same way as in the conforming case is not possible since the function z_h is discontinuous in the vertices. Using the conforming 'dual solution' z_h^C which can be easily obtained by the interpolation of z_h as explained before, we perform the same patchwise biquadratic interpolation of z_h^C as in the conforming case. In fact, the computed nonconforming dual solution z_h is postprocessed twice to get z^I.
Another way of defining $\tilde{z}$ is computing the dual problem with higher order elements. In this paper, we denote by $z^{(2)}$ the solution of the dual problem computed with conforming biquadratic elements on the same mesh as the primal problem. By this, one gets a much more accurate approximation of z than z^I, but on the other hand the computation of the dual problem, which is in fact an auxiliary problem, will dominate the primal problem with respect to computational cost. In this case, z_h^C is defined as the elementwise bilinear interpolation of $z^{(2)}$.

To evaluate the additional term $([u_h], \partial_{\mathfrak{n}} z)_{\partial T}$, we replace z by the arithmetic mean of z_h on the two elements adjacent to the current edge to integrate over

$$\partial_{\mathfrak{n}} z(x) \approx \overline{\partial_{\mathfrak{n}} z}(x) := \frac{1}{2}\Big(\partial_{\mathfrak{n}} z_h|_{T_1}(x) + \partial_{\mathfrak{n}} z_h|_{T_2}(x)\Big), \quad x \in T_1 \cap T_2. \tag{29}$$

By doing so, we obtain the following Lemma:

Lemma 3.1 *For arbitrary $T \in \mathbb{T}_h$, there holds* $\Big([u_h], \overline{\partial_{\mathfrak{n}} z}\Big)_{\partial T} = 0.$

Proof: $z_h|_{T_1}$ und $z_h|_{T_2}$ are linear. Therefore, $\partial_{\mathfrak{n}} z_h|_{T_1} - \partial_{\mathfrak{n}} z_h|_{T_2}$ is constant and $[u_h] \cdot \frac{1}{2}(\partial_{\mathfrak{n}} z_h|_{T_1} - \partial_{\mathfrak{n}} z_h|_{T_2})$ is linear. As u_h is continuous in the midpoints, for a midpoint holds $[u_h](m_\Gamma) = 0$. As the midpoint rule integrates linear functions exactly, we obtain on the edge Γ

$$\int_\Gamma [u_h] \overline{\partial_{\mathfrak{n}} z}\, ds = [u_h](m_\Gamma) \cdot \overline{\partial_{\mathfrak{n}} z}(m_\Gamma) = 0.$$

This completes the proof. □

Since u_h is a piecewise linear function, there holds $\Delta u_h = 0$ on each element such that we get the final error estimation

$$|J(e_h)| \approx \eta(e_h) := \left| \sum_{T \in \mathbb{T}_h} (f, \tilde{z} - z_h^C)_T - \frac{1}{2}([\partial_{\mathfrak{n}} u_h], \tilde{z} - z_h^C)_{\partial T} \right|. \tag{30}$$

In the following, we will denote the error estimator defined by replacing z as z^I by η^I and the error estimator obtained by replacing z by $z^{(2)}$ as $\eta^{(2)}$. To evaluate the quality of the proposed method, we estimate numerically the point error in $(0.5, 0.5)$ in the situation of Test Problem 2.1 on the grid in Figure 2 with regular refinement and distortion after refinement (compare Fig. 3). As a quantitative measure for the quality of the error estimators we define the *efficiency index*

$$I_{\text{eff}} := \frac{\eta(e_h)}{|J(e_h)|}. \tag{31}$$

The numerical results are collected in Tables 4 and 5. The asymptotic exactness promised by $z^{(2)}$ is not observed, as in the third term in the error representation (21) z is replaced by z_h^C instead of $z^{(2)}$. The reason for us to do so is that in this case the third term vanishes completely and therefore it is possible to reuse all programming code written for the conforming case without any additional routine. However, the behaviour of the simple variant η^I for the situation of the non-regular refinement procedure presented (here: via stochastic pertubation) and fine mesh widths is not completely clear while the expensive $\eta^{(2)}$ behaves robust. This is part of our recent work to examine the optimal treatment of the dual solution.

NEL	$\left\|J^r_{(0.5,0.5)}(e_h)\right\|$	$\eta^I(e_h)$	I_{eff}	$\eta^{(2)}(e_h)$	I_{eff}
56	$6.59 \cdot 10^{-4}$	$1.08 \cdot 10^{-3}$	1.64	$3.20 \cdot 10^{-4}$	0.49
224	$1.06 \cdot 10^{-4}$	$2.10 \cdot 10^{-4}$	1.98	$7.47 \cdot 10^{-5}$	0.70
896	$2.63 \cdot 10^{-5}$	$5.87 \cdot 10^{-5}$	2.23	$1.76 \cdot 10^{-5}$	0.67
3584	$6.66 \cdot 10^{-6}$	$1.58 \cdot 10^{-5}$	2.37	$4.23 \cdot 10^{-6}$	0.63
14336	$1.68 \cdot 10^{-6}$	$4.07 \cdot 10^{-6}$	2.42	$1.03 \cdot 10^{-6}$	0.61
57344	$4.23 \cdot 10^{-7}$	$1.02 \cdot 10^{-6}$	2.41	$2.56 \cdot 10^{-7}$	0.60

Table 4
Test Problem 2.1 using the grid in Figure 2, estimation of the point error in $(\frac{1}{2}, \frac{1}{2})$

NEL	$\left\|J^r_{(0.5,0.5)}(e_h)\right\|$	$\eta^I(e_h)$	I_{eff}	$\eta^{(2)}(e_h)$	I_{eff}
56	$6.60 \cdot 10^{-4}$	$1.01 \cdot 10^{-1}$	15,3	$3.20 \cdot 10^{-4}$	0.48
224	$1.03 \cdot 10^{-4}$	$2.13 \cdot 10^{-4}$	2.08	$8.05 \cdot 10^{-5}$	0.78
896	$2.63 \cdot 10^{-5}$	$8.25 \cdot 10^{-5}$	3.13	$1.81 \cdot 10^{-5}$	0.69
3584	$6.69 \cdot 10^{-6}$	$1.35 \cdot 10^{-5}$	2.02	$4.24 \cdot 10^{-6}$	0.63
14336	$1.66 \cdot 10^{-6}$	$4.41 \cdot 10^{-6}$	2.65	$1.05 \cdot 10^{-6}$	0.63
57344	$4.31 \cdot 10^{-7}$	$2.32 \cdot 10^{-6}$	5.38	$2.45 \cdot 10^{-7}$	0.57

Table 5
Test Problem 2.1 using the grid in Figure 2 with distortion after refinement, estimation of the point error in $(\frac{1}{2}, \frac{1}{2})$

Furthermore, we consider the 'square in the channel' which is displayed in Figure 4 ($\Omega = (0,2) \times (0,1) \setminus [0.4, 0.6]^2$). Here, we estimate the point error in $(0.35, 0.5)$ located near the front of the square, i.e. $J(\varphi) = \varphi(0.35, 0.5)$. We choose f and the Dirichlet boundary conditions such that the exact solution u is the same as in Test Problem 2.1. The results are displayed in Table 6. In this special situation, the additional work for $z^{(2)}$ does not lead to an improved estimate of the point error. This is due to the evaluation of the third term, but probably also due to the fact that z is not as smooth as it is required to obtain full convergence with biquadratic elements. This needs $z \in H^3$, but in the case of a non-convex domain even $z \in H^2$ does not have to be valid. Nevertheless, both approaches lead to good estimations of the desired error quantity.

As a third example we use the DFG-benchmark grid 'flow around a cylinder' (Figure 5) and estimate the error in $(0.28, 0.2)$ shortly behind the cylinder. Here, we prescribe the constant right hand side $f = 10$ and homogeneous Dirichlet boundary conditions. As the exact solution is not known, we refer to a reference solution computed with conforming biquadratic finite elements on a very fine mesh (Table 7). The error coming from the approximation of the curved boundary in the case of the cylinder in a channel is neglected here. In

NEL	$\left\vert J^r_{(0.35,0.5)}(e_h)\right\vert$	$\eta^I(e_h)$	I_{eff}	$\eta^{(2)}(e_h)$	I_{eff}
68	$1.97 \cdot 10^{-4}$	$2.13 \cdot 10^{-3}$	10.8	$5.54 \cdot 10^{-4}$	2.81
272	$2.00 \cdot 10^{-4}$	$4.70 \cdot 10^{-4}$	2.35	$1.49 \cdot 10^{-4}$	0.74
1088	$5.86 \cdot 10^{-5}$	$9.65 \cdot 10^{-5}$	1.65	$3.61 \cdot 10^{-5}$	0.62
4352	$1.51 \cdot 10^{-5}$	$2.31 \cdot 10^{-5}$	1.53	$9.93 \cdot 10^{-6}$	0.59
17408	$3.80 \cdot 10^{-6}$	$5.73 \cdot 10^{-6}$	1.51	$2.23 \cdot 10^{-6}$	0.59
69632	$9.51 \cdot 10^{-7}$	$1.43 \cdot 10^{-6}$	1.51	$5.57 \cdot 10^{-7}$	0.59

Table 6
Point error in $(0.35, 0.5)$ using the grid in Figure 4 (square in the channel)

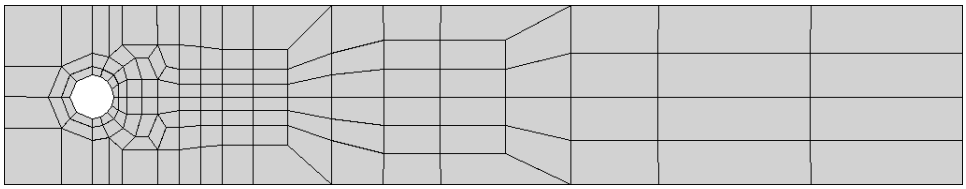

Fig. 5. Grid for DFG-benchmark 'flow around cylinder'

NEL	$\left\vert J^r_{(0.28,0.2)}(e_h)\right\vert$	$\eta^I(e_h)$	I_{eff}	$\eta^{(2)}(e_h)$	I_{eff}
520	$3.56 \cdot 10^{-4}$	$1.10 \cdot 10^{-3}$	3.10	$6.49 \cdot 10^{-4}$	1.82
2080	$9.24 \cdot 10^{-5}$	$3.24 \cdot 10^{-4}$	3.51	$1.63 \cdot 10^{-4}$	1.76
8320	$2.22 \cdot 10^{-5}$	$7.82 \cdot 10^{-5}$	3.52	$4.03 \cdot 10^{-5}$	1.81
33280	$5.35 \cdot 10^{-6}$	$1.97 \cdot 10^{-5}$	3.69	$9.99 \cdot 10^{-6}$	1.87

Table 7
Point error in $(0.28, 0.2)$, 'DFG-benchmark' grid

this situation, the error estimation clearly benefits from taking $z^{(2)}$ instead of z^I. But also the cheaper estimator η^I leads to satisfactory results.

Furthermore, we will estimate the error of the integral of the normal derivative on the interior boundary which is related to the functional J_Γ. This kind of error quantity resembles output functionals like lift and drag coefficients in the case of CFD simulations. The evaluation of the functional $J_\Gamma(T)$ where T represents the temperature is equivalent to the computation of the *Nusselt number* in thermodynamics (compare with [14]). For the corresponding results see Tables 8 and 9.
These results indicate that reliable and efficient error control is possible also for the nonconforming $\tilde{P}_1$-approach. Note that this is true also for the multiply connected domains, where we used the implicit boundary treatment. Although we cannot justify that we neglected the consistency error in this case, the error estimation leads to satisfactory results. On the other hand, this type of error control is not for free as the computation of the dual problem has

NEL	$\lvert J_\Gamma(e_h)\rvert$	$\eta^I(e_h)$	I_{eff}	$\eta^{(2)}(e_h)$	I_{eff}
272	$1.18 \quad 10^{-3}$	$3.47 \quad 10^{-3}$	2.94	$1.80 \cdot 10^{-3}$	1.52
1088	$5.59 \quad 10^{-4}$	$1.35 \quad 10^{-3}$	2.41	$8.02 \cdot 10^{-4}$	1.43
4352	$3.12 \quad 10^{-4}$	$5.27 \quad 10^{-4}$	1.69	$3.78 \cdot 10^{-4}$	1.21
17408	$1.67 \quad 10^{-4}$	$2.21 \quad 10^{-4}$	1.33	$1.84 \cdot 10^{-4}$	1.10
69632	$8.63 \quad 10^{-5}$	$9.91 \quad 10^{-5}$	1.15	$9.05 \cdot 10^{-5}$	1.05

Table 8
Error estimation for the line integral for the 'square in the channel'

NEL	$\lvert J_\Gamma(e_h)\rvert$	$\eta^I(e_h)$	I_{eff}	$\eta^{(2)}(e_h)$	I_{eff}
520	$4.52 \quad 10^{-2}$	$1.13 \quad 10^{-1}$	2.50	$4.34 \cdot 10^{-2}$	0.96
2080	$2.34 \quad 10^{-2}$	$1.53 \quad 10^{-2}$	0.65	$2.38 \cdot 10^{-2}$	1.01
8320	$1.14 \quad 10^{-2}$	$2.96 \quad 10^{-3}$	2.61	$1.23 \cdot 10^{-2}$	1.09
33280	$5.16 \quad 10^{-3}$	$1.75 \quad 10^{-3}$	3.39	$6.26 \cdot 10^{-3}$	1.21

Table 9
Error estimation for the line integral for 'flow around a cylinder'

approximately the same numerical cost as the computation of the problem itself and, therefore, applying the dual weighted residual based error control presented here doubles, at least, the total computational costs as shown by the results in Table 10 which contains the CPU times for the example of the point error estimation in the situation of the 'square in the channel' presented above. In our experiments, we use a Compaq ALPHA with 667 MHz. As solver, we take BiCGStab with ILU(1) as preconditioner. The preconditioner is taken from SPLib [4]. As the numerical amount of the iterative solver used here grows like $N^{1.5}$ where N denotes the number of unknowns, the computational time grows by a factor eight per refinement. The results show that the numerical amount for the primal and dual problem is almost the same. However, one should keep in mind that the growth of computational time coming from the error estimation can be compensated by adapting the grid locally to the desired user-specific quantity, so that instead of applying regular refinement we can refine the computational grid selectively as shown in the papers of Becker and Rannacher. In the presented work we still restrict to regular refinement.

4 Summary and Outlook

After a short introduction of the new linear nonconforming finite element $\tilde{P}_1$, we reviewed the dual-weighted residual based method of error estimation in the sense of Becker and Rannacher. This method allows to measure the error

NEL	primal problem	dual problem	CPU time
17408	3.9 (96)	4.0 (112)	7.9
69632	22.2 (218)	37.2 (246)	59.4
278528	290 (469)	322 (596)	612

Table 10
Computational times in seconds (number of iteration steps) for the primal and dual problem in the case of the square in the channel, η^I, BiCGStab with ILU(1) and resorting

with respect to quite general target functionals. Displaying differences and similarities to the conforming case we transferred this method to the nonconforming $\tilde{P}_1$-element which plays in this context the role of a protypical nonconforming element because of its extraordinary simplicity. Several numerical examples show the reliability and accuracy of this kind of error estimation also in the nonconforming case, although the theoretical foundation of the proposed methods is still not fully clear, as we need $z \in H^2(\Omega)$, which is not realistic in the case of the square in the channel, where the method performed well, too. The additional effort induced by numerically solving the dual problem seems to be the price to pay for the flexibility of choosing an arbitrary target functional in the error estimation.
The new element $\tilde{P}_1$ examined here has the major drawback not to be LBB-stable as shown in [7] which makes it an unsuitable element for CFD. If this problem is overcome, $\tilde{P}_1$ might be a promising candidate for solving saddle-point problems like the incompressible Navier-Stokes equation because of its extraordinary simplicity combined with approximation properties comparable to those of common low order elements.

References

[1] Arnold, D.N, Boffi, D., and Falk, R.S. Approximation by quadrilateral finite elements. *Math Compt.*, 71(239):909–922, 2002.

[2] Becker, R. and Rannacher, R. An optimal control approach to a posteriori error estimates in finite element methods. In *Acta Numerica 2001*, pages 1–102. Cambridge University Press.

[3] Becker, R. and Rannacher, R. A feed-back approach to error control in finite element methods: Basic analysis and examples. *East-West J. Numer. Math*, 4, 1996.

[4] Bramley, R. and Wang, X. Splib: A library of iterative methods for sparse linear systems, 1995.

[5] Buijssen, S.H.M. and Turek, S. Sources of parallel inefficiency for incompressible CFD simulation. In Monien, B. and Feldmann, R., editors, *Proceedings 8th*

International Euro-Par Conference, LNCS. Springer, January 2002. Paderborn, Germany, August 27-30.

[6] Grajewski, M. Numerische Analyse einer nichtkonformen linearen Finite-Elemente-Methode auf Viereckgittern. Diploma thesis, May 2003. University of Dortmund.

[7] Grajewski, M., Hron, J., and Turek, S. Numerical analysis and a-posteriori error control for a new nonconformining linear finite element on quadrilaterals. Technical report, University of Dortmund, Vogelpothsweg 87, 44227 Dortmund, August 2003.

[8] Kanschat, G. and Suttmeier, F.-T. A posteriori error estimates for nonconforming element schemens. *Calcolo*, 36:129–141, 1999.

[9] Park, C. *A study on locking phenomena in finite element methods*. PhD thesis, Seoul National University, 2002.

[10] Park, C. and Sheen, D. P_1-nonconforming quadrilateral finite element methods for second order elliptic problems. *SIAM J. Numer. Anal.*, 41:624–640, 2003.

[11] Schieweck, F. A posteriori error estimates with post-processing for nonconforming finite elements. *Comput. Methods Appl. Mech. Eng.*, 36:489–503, 2002.

[12] Turek, S. *Efficient solvers for incompressible flow problems: An algorithmic and computational approach*. Springer, 1999.

[13] Turek, S. and Rannacher, R. A simple nonconforming quadrilateral Stokes element. *Numer. Meth. Part. Diff. Equ.*, 8:97–111, 1992.

[14] Turek, S. and Schmachtel, R. Fully coupled and operator-splitting approaches for natural convection. *Int. Numer. Meth. Fluids*, 40:1109–1119, January 2002.